



HAL
open science

Control influence on electromagnetic generator pre-design for wave energy converter

Marie Ruellan, Hamid Ben Ahmed, Bernard Multon, Aurélien Babarit, Alain
H. Clément

► **To cite this version:**

Marie Ruellan, Hamid Ben Ahmed, Bernard Multon, Aurélien Babarit, Alain H. Clément. Control influence on electromagnetic generator pre-design for wave energy converter. International Conference on Electrical Machines 2006, Sep 2006, CHANIA, Greece. 7p. hal-00676121

HAL Id: hal-00676121

<https://hal.science/hal-00676121>

Submitted on 3 Mar 2012

HAL is a multi-disciplinary open access archive for the deposit and dissemination of scientific research documents, whether they are published or not. The documents may come from teaching and research institutions in France or abroad, or from public or private research centers.

L'archive ouverte pluridisciplinaire **HAL**, est destinée au dépôt et à la diffusion de documents scientifiques de niveau recherche, publiés ou non, émanant des établissements d'enseignement et de recherche français ou étrangers, des laboratoires publics ou privés.

Control influence on the electromagnetic generator pre-design for a wave energy converter

M. Ruellan, H. Ben Ahmed, B. Multon, A. Babarit*, A.H. Clément*
 SPEELabs/SATIE – Brittany Branch Campus (UMR CNRS 8029), ENS de Cachan
 * LMF, Ecole Centrale de Nantes (UMR CNRS 6598)
 e-mail: ruellan@bretagne.ens-cachan.fr

Abstract — We will report herein on three control strategies and the pre-design methodology of an electromagnetic generator for wave energy recovery. We will start by describing the wave energy converter (WEC) concept studied within the context of the SEAREV project [1]. Power takeoff (PTO: the generator) behavior results from strong coupling between hydrodynamic, mechanical and electrical phenomena, leading to a complex device design problem. We will also present the three pertinent control methods. A design methodology has been laid out on a swell cycle that, despite being of limited duration, is representative of the study problem.

Keywords: optimization, control, design methodology, direct drive generator, wave energy converter.

I. INTRODUCTION

Swells represent a major renewable energy resource (an average of 320 GW in Europe or the equivalent of 2,800 TWh). Recovering just a small portion of wave energy would make a significant contribution to meeting electrical energy production needs and only cause minimal environmental impact with very limited greenhouse gas emissions over the course of the life cycle.

Swells however display the characteristic of being highly fluctuating and non-periodic. The WEC concept is based on a pendulum set in a closed buoy actuated by the swell through excitation forces [2] (see Fig. 1). The pendulum executes rotational movements transmitted to the rotor of an electromagnetic generator (itself coupled to a load via an electronic power converter), which recovers a portion of its kinetic energy. To a certain extent, this set-up constitutes an active recovery damper.

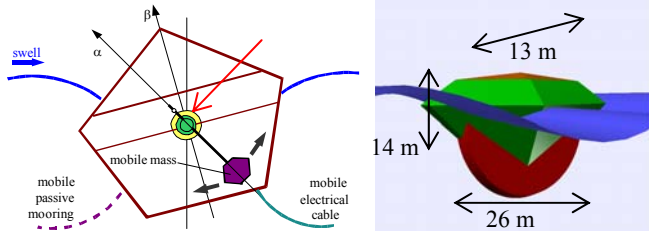


Figure 1a: Conceptual diagram of the pendular wave energy converter

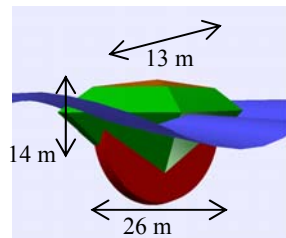


Figure 1b: Primary dimensions of the full scale SEAREV prototype design

The design of a generator adapted to swells must, first and foremost, take into account the nature of loadings, and in particular their complexity. The sizing and optimization of

such a system thus requires incorporating the relatively strong coupling existing between physical phenomena: hydrodynamics - mechanics - electricity - control. In an initial approach, the electromechanical part can be modeled by means of a simplified recovery function that strictly pertains to a recovery torque whose form (whether analytical or numerical) has been optimized in the aim of obtaining, under given excitation conditions, maximum recovered electrical energy.

II. MECHANICAL AND HYDRODYNAMIC MODEL

The recovered electrical power computation requires determining movements of the coupled device {buoy + pendulum + generator with control}. A multi-physical hydrodynamic-mechanical-electrical model now needs to be derived.

The general equation to be solved is of the following form:

$$M \cdot \ddot{X} = \sum F_{\text{ext}} \quad (1)$$

where M represents the system's inertia matrix and $X = [x_G \ z_G \ \theta \ \alpha]$ is the displacement vector (see Fig. 2).

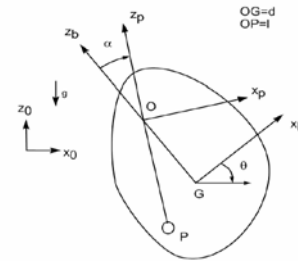


Figure 2: Coordinate systems and notations employed

F_{ext} is the generalized forces vector:

$$F_{\text{ext}} = F_p + T_R + F_H + F_R + F_{\text{ex}} \quad (2)$$

F_p represents the force exerted by the pendulum at point O. This force depends upon X , \dot{X} and the set of geometric parameters of both the buoy and pendulum (see Appendix A).

F_H stands for the hydrostatic force due to buoyancy.

F_R is the so-called radiation force corresponding to the reaction of the {buoy + pendulum} system on the swell.

T_R is the energy recovery torque exerted by the electromagnetic generator, with its value stemming from an optimized control strategy that will be discussed further below.

Swell excitation forces, F_{ex} , are calculated from a set of imposed swell resources for a given overall buoy geometry. A

swell is characterized by its significant height (i.e. crest-to-trough), denoted $H_{1/3}$ and its peak period T_1 .

In the case of the simplified system set-up herein, just three swell force components on the buoy merit our attention: the horizontal force F_{ex_X} (surge), vertical force F_{ex_Z} (heave), and y -axis moment (pitch) F_{ex_θ} .

III. DESIGN METHODOLOGY

The system is submitted to a fluctuating and previously-characterized swell. In order to recover the maximum amount of energy, various elements need to be optimized, starting with the hydrodynamic shape of the buoy, the electromagnetic generator and the control strategy [2]. The coupling between all elements is strong, yet it is initially sought to handle the generator design problem from a decoupled perspective. The generator will in fact be treated like a device capable of imposing a braking torque. The reaction of this braking torque on both the buoy and swell is still to be taken into account by the model.

On the basis of these excitation forces and in accordance with a hydrodynamic-mechanical-electrical multi-physical model, the power and recovered electrical energy are calculated at each point in time over a fixed period ΔT ($\Delta T \gg T_1$) long enough to make the pendulum startup time remain negligible. The generator's electrical behavior (active damper of the pendulum) directly influences the recovered energy value in addition, by means of coupling, to the dynamics of the buoy-pendulum system.

The optimization step consists of seeking the law of instantaneous electromagnetic torque variation $T(t)$ that maximizes recovered energy and minimizes the peak power. The diagram below illustrates this optimization methodology.

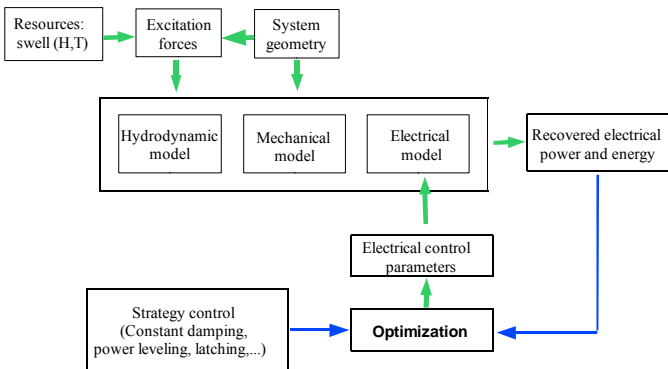


Figure 3: Design synopsis of a swell generator [3]

In this article, we will present three control methods:

- optimization of the viscous and recovery damping coefficient β ,
- a method for leveling the power, and
- a so-called latching method.

These three methods will be more closely examined in the following sections.

A. Optimization with constant recovery coefficient β

Given that the search in this setting for a temporal evolution in the torque exerted by the generator constitutes a complex problem by the number of optimization variables

required, we have deliberately opted for a "progressive" approach, which consists of imposing the general shape of the torque, of the viscous damping type:

$$T_R(t) = \beta \dot{\theta}(t) \quad (4)$$

where β is the viscous damping coefficient, which remains constant over the full cycle period (including during the transient pendular motion start-up phase). The optimization problem then becomes one of seeking the values of β such that the recovered mechanical energy W_e (given in (5)) is maximized.

$$W_e = \int_{\Delta t} \beta [\dot{\theta}(t)]^2 dt \quad (5)$$

Figure 4 presents a sample profile of the instantaneous recovered power for a swell with a 10-sec period and 6-m height, for which the overall dimensions have been listed in Appendix A.

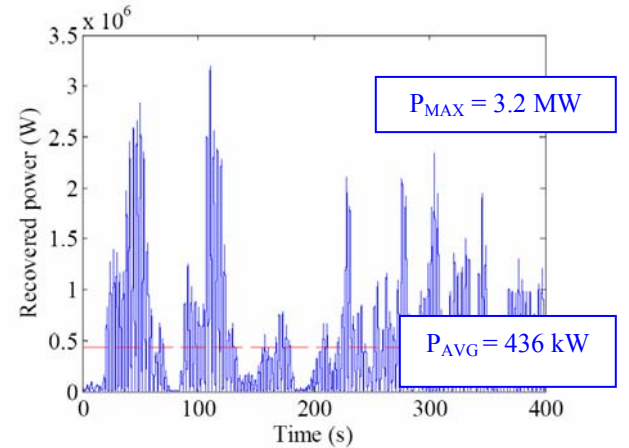


Figure 4: Recovered power with constant β_{opt} during the full cycle

The optimal value of recovery coefficient β_{opt} varies depending on the type of swell acting upon the system. We will present below, in the form of a scatter diagram, the average recovered power levels (Fig. 5) along with the corresponding optimal values of recovery coefficient β_{opt} (Fig. 6) for various types of swells (simulations conducted on 400-sec cycles).

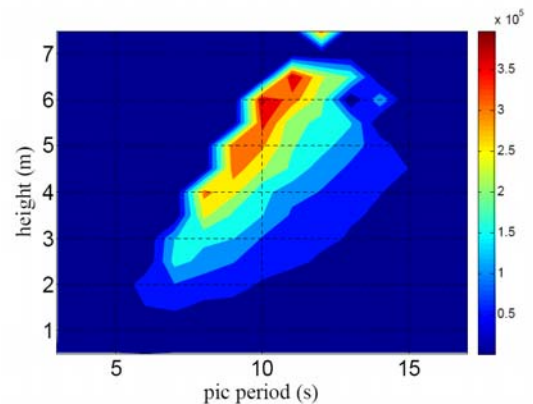


Figure 5: Scatter diagram of recovered power (W) with constant β_{opt}

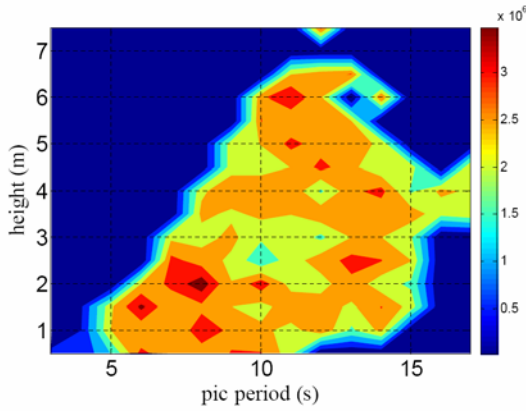


Figure 6: Scatter diagram of optimal recovery coefficient (Nms/rad) corresponding to Figure 5

B. Optimization with power leveling

The previously-described control strategy is implemented here solely on the power maximization criterion. The instantaneous recovered power displays sizable fluctuations (see Fig. 4); these in turn lead to an over-designed electrical conversion system. Using the swell example provided above (Fig. 4), we obtain an average power level of 436 kW and a peak power of 3.2 MW for a damping coefficient $\beta_{opt} \cong 3$ MNms/rad. Leveling the converted power (as practiced on an eolian system) would facilitate economic profitability optimization.

In our specific case, this leveling is obtained by means of modifying (reducing) the value of the recovery damping coefficient β . For those phases in which the power lies below the imposed leveling power, the value of β is held constant (generator operating with a torque of the viscous friction type), optimized in the aim of maximizing average power. For those phases in which the power generated is greater than the leveling power, the damping coefficient β varies temporally such that the power generated remains equal to the leveling power (generator operating at constant power). This strategy has been illustrated by Equation 6.

$$\beta(t) = \begin{cases} \beta_{opt} & \text{for } P(t) \leq P_{lev} \\ \frac{P_{lev}}{\dot{\theta}^2} & \text{for } P(t) > P_{lev} \end{cases} \quad (6)$$

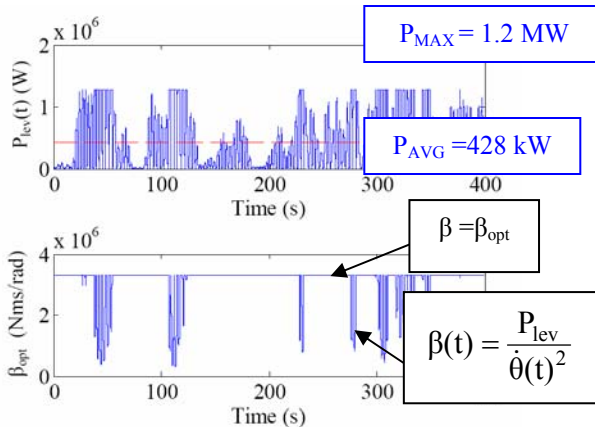


Figure 7: Recovered power after power leveling (40%) and the corresponding damping coefficient

A sample of the results obtained under the same conditions as before is shown in Figure 7.

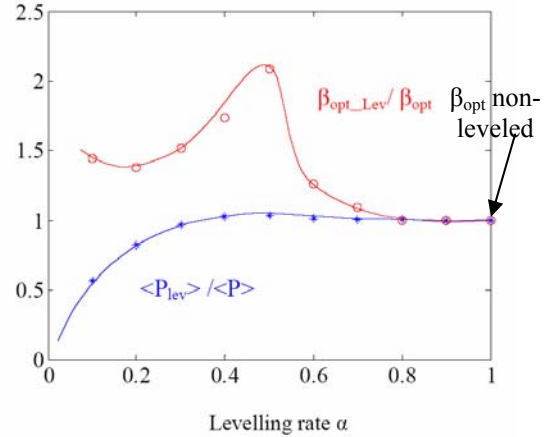


Figure 8: $\langle P \rangle / P_{lev}$ ratio in leveling mode corresponding to the leveling ratio (*blue) and $\beta_{opt_lev} / \beta_{opt}$ corresponding to the leveling ratio (° red)

Figure 8 presents the ratio of average leveled-recovered power to the average non-leveled recovered power ($\alpha=1$) as well as the ratio of optimized damping coefficient with leveling to the optimized damping coefficient without leveling ($\alpha=1$). These results highlight the efficiency of the leveling strategy in spite of its simplicity (a constant recovery coefficient β over the full cycle outside of the leveling zones). The leveling step enables imposing higher damping coefficients β without any significant power loss. The average recovered powers in fact remain substantial for a leveling rate α of above 20%.

C. Optimization with latching control [4]

Latching control consists of locking (latching) the motion of the body at the instant when its velocity vanishes, while waiting for the wave force to have reached the optimal phase for releasing the body. The body then starts moving from this initial position to the next vanishing velocity position, where it is latched again, and so forth and so on. Instead of being a smooth, continuous function, the position of the body is a succession of transient motion ramps separated by resting stages. The action upon the system is therefore binary: either the body is latched, or it is free to move (Equation 7 and Fig. 9).

$$W_e = \int \beta \dot{\theta}(t)^2 (1 - u(t)) dt \quad (7a)$$

$$\text{With: } u(t) = \begin{cases} 1 \\ 0 \end{cases} \quad (7b)$$

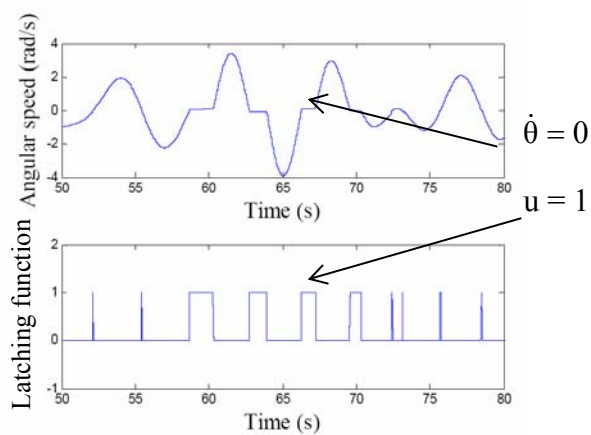


Figure 9: Example of angular speed and latching function (zoom)

The instant of latching is imposed by the dynamics of the body itself (i.e. vanishing velocity); thus, the control variable is simply the duration of the latching phase Δt , or equivalently the instant of release. This mode of control, applied to the heave motion of the buoy, was proposed by Budal and Falnes [5].

Figure 10 provides an example of results obtained under the same conditions as for the two other strategies with latching control.

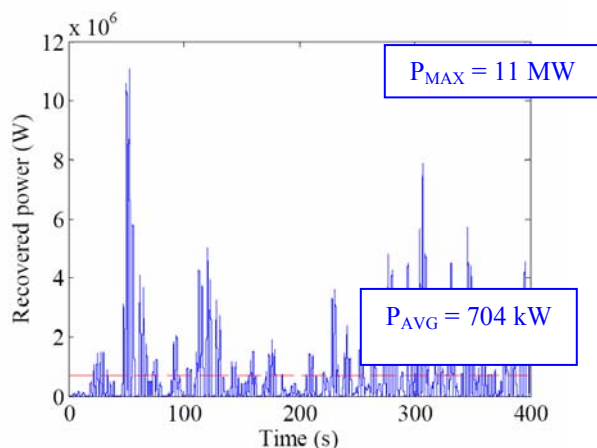


Figure 10: Recovered power with latching control

D. Assessment of the methods proposed

Table 1 summarizes the results obtained for the three control modes presented above. It may be observed that the average recovered power is higher for the latching mode, which is explained by an increase in the pendulum's rotational velocity. The ratio of average power-to-peak power is nonetheless heavily deteriorated; we note a very high peak power in the case of the latching mode that causes the "power electronics" part to be over-designed.

When leveling, the peak power decreases substantially and an improved design is derived for both the converter and all electrical network components. This power optimization strategy does entail however incurring production losses.

TABLE 1: SUMMARY PRESENTATION OF RESULTS

| | β constant over cycle | Power leveling | Latching |
|---|--------------------------------|-------------------|----------|
| Average power (kW) | 436 | 428 | 704 |
| Maximum power (MW) | 3.2 | 1.2 | 11 |
| Ratio of average-to- maximum power (%) | 13.6 | 6.3 | 33.8 |
| Maximum torque (MNm) | 3.1 | 2 | 2.6 |
| RMS torque (MNm) | 1.15 | 1 | 0.7 |
| Maximum speed (rad/s) | 1.0 | 1.9 | 4.1 |

IV. PRE-DESIGN OF A PM SYNCHRONOUS MACHINE

We have undertaken the preliminary design of the generator on the basis of results obtained on a reduced-duration swell cycle in order to evaluate in particular the realism of direct drive.

The generator considered for this preliminary design is of a conventional synchronous structure with surface magnets cylindrically-shaped with a radial field and an internal rotor [6]. This initial study enables refining the optimization approach and tools devised and then generates some qualitative results, while strictly adhering to the set of specifications developed for this device.

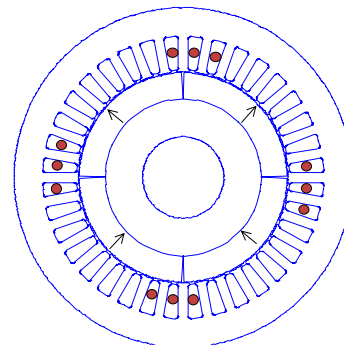


Figure 11: Generator architecture: a synchronous machine with radial flux and mounted surface magnets

1) Formalism

The goal herein is to determine the set of optimal geometric characteristics for the synchronous generator that enable minimizing, from a Pareto perspective, two competing objectives: total losses and the volume (or mass) of active parts. This procedure is carried out by focusing on the torque $T_R(t)$ and rotational speed $\Omega(t)$ obtained during the previous systems optimization steps over a given operating cycle (see Figs. 12, 13 and 14).

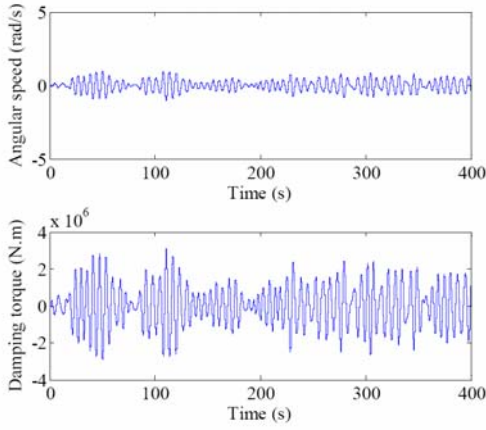
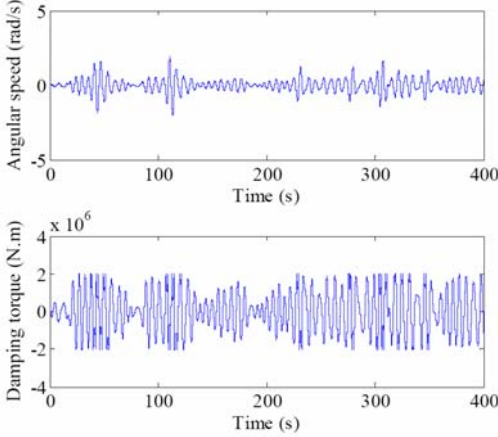
Figure 12: Speed and torque profiles (with constant β_{opt} over the cycle)

Figure 13: Speed and torque profiles (with power leveling (40%))

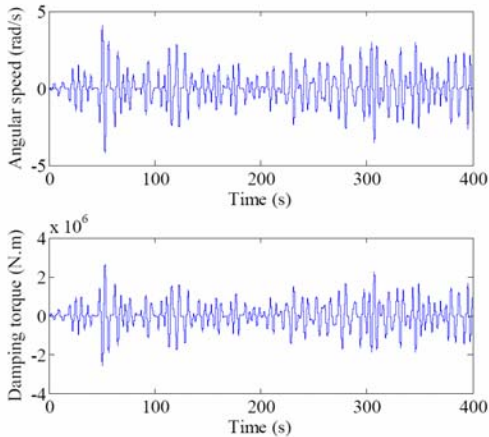


Figure 14: Speed and torque profiles (with latching control)

By introducing a few simplifications (infinite iron permeability, model limited to the first harmonic, surface cooling), the efficient line density variation for armature current A_{Leff} required to generate the desired torque profile is given by:

$$A_{Leff}(t) = \frac{T_R(t)}{k} \quad (7)$$

where k represents the torque constant given by:

$$k = 2\sqrt{2}K_B b_{fmax} V_r \cos(\psi) \quad (8)$$

where K_B is the winding coefficient, ψ the EMF-current dephasing and $V_r = \pi(R)^2 \cdot L$ is the rotor displacement.

B_{fmax} is the amplitude of the airgap induction fundamental due to the inductor with surface magnets (in neglecting the curvature effect) and may be approximated by:

$$B_{fmax} = \frac{4}{\pi} \frac{M}{1 + \frac{K_c e}{l_a}} \sin\left(p \frac{\beta_a}{2}\right) \quad (9)$$

where M is the saturation magnetization of magnets, β_a the relative magnet opening ($\beta_a=1$ for contiguous magnets), K_c represents the Carter coefficient (with e being the mechanical clearance) and K_r the inter-magnetic leakage coefficient :

$$K_r \cong \frac{3p\beta_a K_c e}{4R} \quad (10)$$

This optimization approach must respect a thermal constraint (maximum temperature rise according to an average model) and two magnetic constraints (demagnetization of magnets and magnetic saturation in the yokes) (see Appendices B and C).

Since rotational speeds are low, only the copper and magnetic losses have been taken into account (see Appendix D).

2) Optimization

This optimization approach makes use of the NSGA-II genetic optimization algorithm [7]. Figure 19 displays its overall structure.

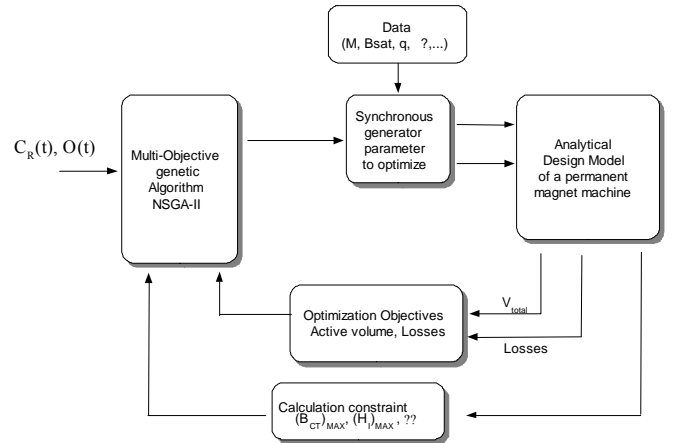


Figure 15: General overview of this generation-based optimization approach

The optimization variables (limited to a few geometric magnitudes in this preliminary design study) are the bore radius R , magnet thickness l_a and relative magnetic angular opening β_a , active machine length L , slot height h_{enc} , internal yoke thickness h_{cui} and external yoke thickness h_{cuc} , the number of pole pairs p , and the speed multiplier ratio in the case of an indirect drive.

We will now present the results obtained for the three control strategies introduced above, i.e. optimization of recovery coefficient β (constant over the full cycle), power leveling ($\alpha=40\%$), and control by means of latching, via both direct and indirect drives.

These results have been displayed in Figures 16 and 17 in the form of a Pareto front.

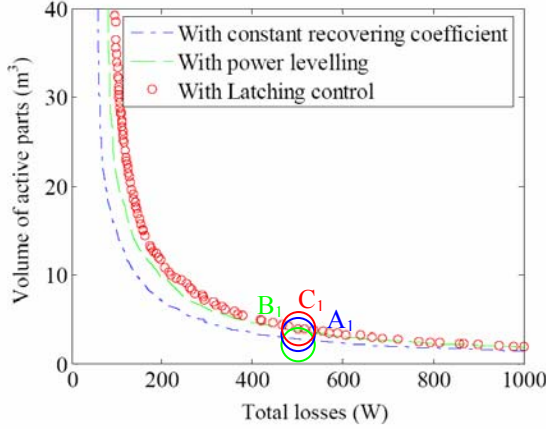


Figure 16: Optimization for the three control strategies in direct drive

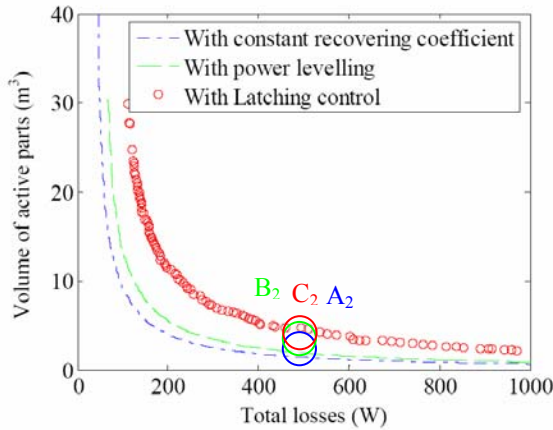


Figure 17: Optimization for the three control strategies in indirect drive

For purposes of illustration, we will compare, for the three control strategies (points A, B and C identified on Figure 18 and in Tables 2 and 3), the optimal machine dimensions (compromise found between the two contradictory objectives) with equal losses (≈ 500 W) for both direct (1) and indirect (2) drive modes. The columns list peak power values.

TABLE 2: OPTIMIZATION RESULTS IN DIRECT DRIVE

| | A ₁ (--) | B ₁ (--) | C ₁ (o) |
|------------------------------------|---------------------|---------------------|--------------------|
| Total active mass (T) | 24 | 32 | 37 |
| Magnet mass (T) | 0.27 | 0.25 | 0.18 |
| Active volume (m ³) | 2.7 | 3.7 | 4.3 |
| External radius (m) | 5.2 | 5.4 | 4.9 |
| Length (m) | 0.1 | 0.1 | 0.1 |
| Number of poles (p) | 148 | 149 | 138 |
| $\langle P_r + P_{mg} \rangle$ (W) | 506 | 504 | 480 |

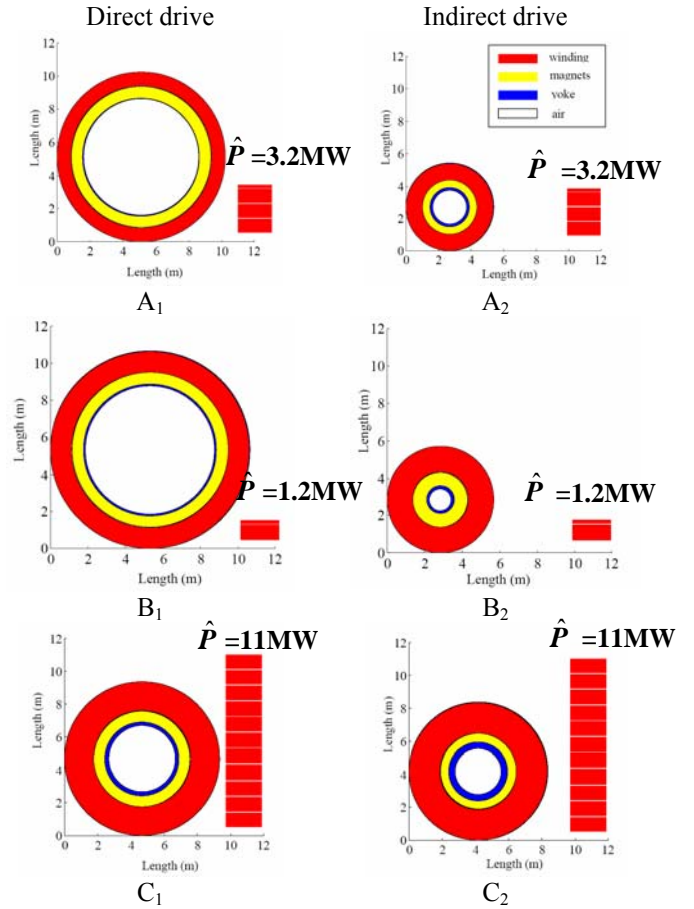


Figure 18: Optimal geometry without (1) and with (2) gearing and employing the various control strategies (A: constant β ; B: power leveling; C: latching)

TABLE 3: OPTIMIZATION RESULTS IN INDIRECT DRIVE

| | A ₂ (--) | B ₂ (--) | C ₂ (o) |
|------------------------------------|---------------------|---------------------|--------------------|
| Total active mass (T) | 13 | 16 | 41 |
| Magnet mass (T) | 0.13 | 0.17 | 0.18 |
| Active volume (m ³) | 1.5 | 1.8 | 4.7 |
| External radius (m) | 2.8 | 2.9 | 4.6 |
| Length (m) | 0.1 | 0.1 | 0.1 |
| Speed multiplier ratio | 5 | 5 | 2 |
| Number of poles (p) | 76 | 69 | 81 |
| $\langle P_r + P_{mg} \rangle$ (W) | 482 | 519 | 495 |

V. CONCLUSION

This article has presented the influence of three types of control strategies on the design of a swell generator.

To conduct this assessment, the *systems* model produced had to include hydrodynamic, electromagnetic and control aspects. Moreover, a cycle optimization sequence was adopted that incorporated the fluctuating nature of the (swell) load. Although further refinements remain necessary, the results of this study have served first to validate the approach and tools implemented. Highlighting the heavy influence of the choice of control strategy on both generator design and the quality of recovered energy then became possible. With respect to the sole criterion of maximizing average recovered power, the *latching* strategy provided greater recovery efficiency for nearly identical active generator part masses. This approach however always entails the sacrifice of a much higher power undulation and hence over-designing the associated electrical

modules (e.g. electronic power converter, network connection systems, buffer storage system). A hybrid control that includes both a *latching* control set-up and a power-leveling strategy shows great promise; this set-up would undoubtedly lead to a quantity / quality compromise between recovered energy and useful active part masses.

Moreover, the architecture of the electromagnetic generator proposed herein is of the conventional synchronous cylindrical type with surface magnets. A comparative study with other generator structures, especially one with double excitation [8], has been planned to include integration constraints in the pendular mechanical system.

APPENDIX A: HYDRODYNAMIC PARAMETER VALUES

| Designation | Symbol | Value |
|---|-------------------------|-----------------------|
| Buoy mass | Mb (kg) | 551,000 |
| Buoy inertia | Ib (kg.m ²) | 0.431 10 ⁸ |
| Pendulum mass | Mp (kg) | 393,000 |
| Pendulum inertia | Ip (kg.m ²) | 4.62 10 ⁶ |
| Length between pendulum rotation center and center of gravity | l (m) | 0.92 |
| Length between buoy rotation center and center of gravity | d (m) | 0.01 |

APPENDIX B: THERMAL CONSTRAINT

$$\frac{1}{\Delta T} \int_{\Delta T} [P_j(t) + P_{mg}(t)] dt \leq \Delta \theta$$

$$\alpha_{th} S_{th}$$

where $S_{th} = 2\pi R_{ext} L$ is the thermal exchange surface corresponding to the machine's external surface.

APPENDIX C: MAGNETIC CONSTRAINTS

$$\frac{R\pi}{Lp} \sqrt{(B_{fmax} + B_{Id_{max}})^2 + B_{Iq_{max}}^2} \leq B_{sat} : \text{saturation}$$

$$\text{with: } B_{Id}(t) = -\frac{3}{2} \sqrt{2} \frac{R}{k_r pq} \sin(\psi) P_{sed} \frac{T_R}{k}$$

$$\text{and: } B_{Iq}(t) = \frac{3}{2} \sqrt{2} \frac{R}{k_r pq} \cos(\psi) P_{seq} \frac{T_R}{k}$$

the airgap induction components due to both the induced and inducing field.

$$\sqrt{2} \frac{K_B \pi R}{pq(K_c e + h_a)} \left(\frac{T_R(t)}{k} \right)_{max} \leq H_K : \text{demagnetization limit}$$

at the target operating temperature.

$$P_{seq} = P_{sed} = \frac{\mu_0}{K_c e}, \text{ the surface airgap permeances in both the } d$$

and q axes.

$$\text{The mechanical airgap } e \text{ is given by: } e = K_c (2 \cdot 10^{-4} + \frac{R}{200}).$$

APPENDIX D: LOSS EXPRESSIONS

The expressions for instantaneous copper and iron losses are set forth in (12) and (13), respectively.

$$P_j(t) = \frac{8}{\pi} \rho \frac{\pi L R K_L}{k_r h_{enc} (1 + \frac{h_{enc}}{2R})} \left(\frac{T_R(t)}{k} \right)^2$$

with: $K_L \cong 1 + \left(\frac{\pi R}{p L} \right)$ being a coefficient that incorporates the winding heads.

$$P_{mg}(t) = [V_c (B_{cr})^2 + V_d (2B_{cr})^2] \times \left(\frac{p}{2\pi} \Omega(t) \right) \left[k_H + k_{cf} \cdot \left(\frac{p}{2\pi} \Omega(t) \right) \right]$$

V_c represents the volume of the stator yoke and V_d the volume of the toothed stator zone.

$$B_{cr} = \left(\frac{\pi R}{p h_c} \right) B_{eT}$$

$$\text{where: } B_{eT} = \sqrt{(B_{fmax} + B_{Id_{max}})^2 + B_{Iq_{max}}^2}$$

APPENDIX E: CONSTANT PARAMETERS

| Designation | Value |
|---|------------------------|
| Magnet magnetization at 20° (M) | 1 T |
| Demagnetization field at 20° (H _K) | 760 kA/m |
| Relative magnetic permeability (μ_{ra}) | 1 |
| Iron saturation induction (B_{sat}) | 1.5 T |
| Hysteresis loss coefficient (k_H) | 90 A.m/V.s |
| Coefficient of Foucault current losses (k_{cf}) | 1.28 A.m/V |
| Copper resistivity at 20°C | 1.8e-8 Ω .m |
| Copper-filling coefficient (k_r) | 0.4 |
| Winding coefficient K_B | 0.956 |
| Carter coefficient K_c | 1.1 |
| Thermal exchange coefficient (α_{th}) | 10 W/m ² .K |
| Phase number (q) | 3 |
| EMF-current dephasing (ψ) | 0° |

REFERENCES

- [1] A.H. Clément *et al.*, French patent, "Autonomous electrical system for wave energy conversion". In French « Système Electrique Autonome de Récupération de l'Energie des Vagues », 2004.
- [2] A. BABARIT: "Hydrodynamic Optimization and optimal control of a wave energy converter". In French, « Optimisation hydrodynamique et contrôle optimal d'un récupérateur d'énergie des vagues. Thesis Centrale Nantes/Université de Nantes, in French, Oct. 2005.
- [3] M. RUELLAN *et al.*, « Pre-design of a pendular wave energy converter ». In French, « Prédimensionnement d'un houlo générateur pendulaire », EF2005, Sept. 05.
- [4] A. BABARIT, G. DUCLOS, A.H. CLÉMENT (2005): Comparison of latching control strategies for a heaving wave energy device in random sea; Applied Ocean Research Vol. 26, 5, pp. 227-238.
- [5] BUDAL K, FALNES J. Interacting point absorbers with controlled motion, in Power from Sea Waves. BM Count: Academic Press; 1980.
- [6] FITAN E., MESSINE F., NOGAREDE B.: "The electromagnetic actuator design problem: a general and rational approach. IEEE Transactions on Magnetics, Volume 40, No. 3, May 2004.
- [7] DEB K., PRATAB A., AGRAWAL S. Heyarivau T. "A Fast and Elitist Genetic Algorithm: NSGA-II ". IEEE Transactions on evolutionary computation, Volume 6, No. 2, pp. 182-197, April 2002.
- [8] AMARA Y *et al.* « A new topology of hybrid synchronous machine » IEEE Transactions on Industry Applications Volume 41, no. 4, pp. 989-995, July-Aug. 2005.